#### **ORIGINAL ARTICLE**



# Artificial intelligence-based modeling of hot deformation behavior in AA 5052-H32 alloy

Rafael Pandolfo da Rocha<sup>1</sup> • Matheus Henrique Riffel<sup>1</sup> • André Rosiak<sup>1</sup> • Luis Fernando Folle<sup>2</sup> • Tiago Nunes Lima<sup>3</sup> • Lirio Schaeffer<sup>1</sup>

Received: 8 July 2025 / Accepted: 25 September 2025 © The Author(s), under exclusive licence to Springer-Verlag London Ltd., part of Springer Nature 2025

#### **Abstract**

This study investigates the application of machine learning techniques to predict the deformation behavior of the AA 5052-H32 aluminum alloy over a wide range of processing conditions. Tensile tests were conducted at different temperatures (100–450 °C) and strain rates (0.01 and 1 s<sup>-1</sup>), enabling the acquisition of the material's flow curves. The experimental data were fitted to the Hensel–Spittel constitutive equation and subsequently employed in the development of Artificial Neural Network (ANN) and eXtreme Gradient Boosting (XGBoost) models. The AI-based models exhibited superior predictive performance compared to the phenomenological approach. The optimized ANN, with a dense architecture consisting of two hidden layers with 256 and 128 neurons, achieved a mean absolute error (MAE) of 3.61 MPa and a mean squared error (MSE) of 19.09 MPa<sup>2</sup>. The XGBoost model, configured with 100 decision trees and a maximum depth of 4, delivered even more accurate results, with MAE of 0.74 MPa, MSE of 2.46 MPa<sup>2</sup>, and a coefficient of determination (R<sup>2</sup>) of 0.9988, showing an almost perfect overlap between predicted and experimental curves. These findings confirm the high accuracy and robustness of machine learning techniques, highlighting their potential as a superior alternative to traditional phenomenological models for predicting flow behavior in forming processes.

**Keywords** Hot forming · Aluminum alloys · Artificial intelligence

## 1 Introduction

Advances in the mobility industry have focused on innovative and economically viable solutions aimed at increasing vehicle energy efficiency. At the same time, requirements related to crash performance have become increasingly stringent. As a result, vehicles are now safer than ever, which has driven the use of lightweight and high-strength materials, carefully selected to meet these demands [1–4].

Rafael Pandolfo da Rocha rafael.pandolfo@ufrgs.br

Published online: 07 October 2025

- Metal Forming Innovation Center (CBCM), Federal University of Rio Grande Do Sul, Porto Alegre, Brazil
- Technical and Industrial School of Santa Maria, Federal University of Santa Maria—UFSM-CTISM, Santa Maria, Brazil
- <sup>3</sup> SENAI CIMATEC, Senai Institute of Innovation for Forming and Joining of Materials (CIMATEC ISI C&UM), Salvador, Brazil

Steel alloys still dominate the automotive sector due to their excellent cost–performance balance. However, aluminum alloys have emerged as a promising alternative to conventional materials, playing a key role in reducing vehicle component weight [5]. These alloys are characterized by high mechanical strength, good energy absorption capacity, high recyclability, and low density, in addition to exhibiting good corrosion resistance [6]. Compared to steel, aluminum alloys enable weight reduction of up to 50% [7].

Over the past decade, the application of aluminum alloys in the automotive industry has increased by more than 80%, a trend expected to intensify as new design concepts advance. In 1996, the average amount of aluminum employed per vehicle was approximately 110 kg; currently, it is estimated that this figure may reach between 250 and 340 kg in the coming years [8]. A notable example is the Audi A8 (2018), whose body structure contains 58% aluminum [9]. Historically, most aluminum products intended for the automotive sector were obtained by casting; however, in recent decades, the stamping of aluminum sheets has gained prominence, especially in the manufacture of external



panels such as hoods and heat shields, as well as structural components such as bumper beams [10].

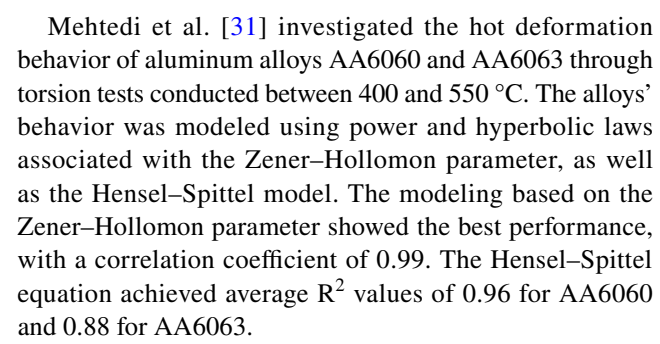
Alloys from the 5xxx and 6xxx series have been widely used in automotive body structures [11–15]. In parallel, the use of high-strength alloys from the 7xxx and 2xxx series—traditionally applied in the aerospace sector—is also under development [16]. Series 5xxx alloys are non-heat-treatable, with strengthening occurring mainly through work hardening. In contrast, 2xxx, 6xxx, and 7xxx series alloys are heat-treatable, allowing strength improvement through aging and precipitation. Regardless of the class, one of the main challenges in forming these materials lies in achieving adequate formability while simultaneously ensuring quality requirements and final part properties [17–19].

To mitigate limitations associated with formability and springback, aluminum alloys traditionally formed at room temperature have been increasingly applied in warm [20–23] and hot stamping processes [24–29]. In these methods, the sheet is heated and subsequently transferred to the press, where it is formed between dies that may be cold, hot, or locally heated [24]. After forming, the part remains in the dies, which reduces the risk of thermal distortions. These approaches allow the production of components with complex geometries and high strength in a single processing step [30].

To achieve such results, processes are carefully analyzed through numerical simulations. In these analyses, the material behavior under plastic deformation constitutes essential information, as the accuracy of numerical models directly depends on the fidelity with which material flow is represented. In hot forming in particular, it is necessary to properly define the relationship between flow stress and thermomechanical parameters of the process. This representation is generally carried out using constitutive equations.

Among the various phenomenological constitutive models, a traditional approach relies on the Zener–Hollomon parameter (Z), which represents the strain rate compensated by temperature. The Arrhenius-type constitutive equation establishes the correlation between this parameter and the flow stress through different mathematical relations: power law, for relatively low stresses; exponential law, for high stresses; and hyperbolic sine law, covering a wide range of deformation conditions [31].

Other constitutive formulations explicitly incorporate the dependence of flow stress on strain. In this group, the strain-dependent Garofalo equations [32–35] and the Hensel–Spittel model [36, 37] are noteworthy. The Garofalo equations represent an evolution of the Arrhenius formulation by including strain as a variable in the constitutive parameters. The Hensel–Spittel model relates flow stress to strain, strain rate, and temperature. It stands out for its concise formulation, ease of calibration compared with other models, and widespread use in commercial finite element software.



New approaches have been developed, particularly by modifying classical models. Liu et al. [29] analyzed the flow behavior of AA6061 at temperatures between 350 and 500 °C and strain rates ranging from 0.01 to 1 s<sup>-1</sup>. For this purpose, modified Arrhenius and Cowper–Symonds equations were applied. The Cowper–Symonds model incorporates the effects of work hardening and strain-rate sensitivity during hot metal forming [38, 39]. Both models demonstrated high accuracy, with average absolute relative errors of 2.90% (modified Arrhenius) and 1.37% (modified Cowper–Symonds).

The hot deformation behavior of AA7046 was analyzed by He et al. [40] using an improved Hensel–Spittel–Garofalo model. This model combines the mathematical structure of Garofalo with strain-dependent parameters, in a manner analogous to the Hensel–Spittel model. The results indicated satisfactory performance, with a coefficient of determination  $R^2$ =0.989.

Despite their accuracy, phenomenological models present certain limitations. Their parameters do not have direct physical meaning, being merely fitting coefficients obtained through regression of experimental data. Consequently, the model is reliable only within the temperature, strain, and strain-rate ranges in which it was calibrated. Outside these ranges, the model may generate unrealistic predictions. This is particularly critical in finite element analyses, as the software may be forced to operate under process conditions not represented in laboratory tests.

As an alternative, the possibility of modeling plastic deformation behavior through artificial intelligence (AI) models has become highly attractive [41–43]. These approaches can capture complex and nonlinear relationships between input and output variables without the need to assume a predefined functional form. Furthermore, they provide greater flexibility in handling large volumes of experimental data and may achieve higher predictive accuracy, even under extrapolation conditions.

Another relevant aspect is that AI models are capable of simultaneously incorporating multiple process variables, which enhances generalization capacity and reduces the limitations observed in purely empirical models.

In this work, artificial intelligence-based approaches were developed to model the plastic behavior of the aluminum



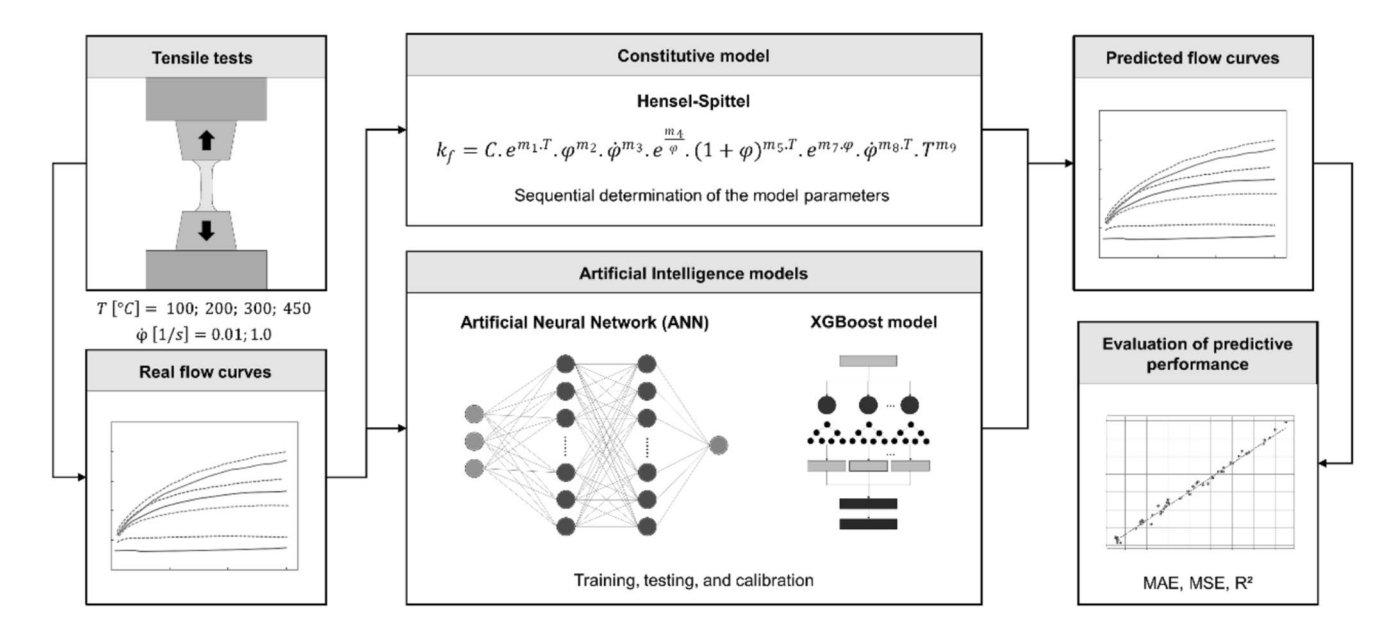


Fig. 1 Schematic representation of the methodological steps adopted in this study

alloy AA 5052-H32, with 1 mm thickness, under warm and hot forming conditions. Flow curves were experimentally obtained at different temperatures and strain rates, serving as the basis for model calibration. eXtreme Gradient Boosting (XGBoost) and Artificial Neural Networks (ANN) algorithms were applied and compared with the classical Hensel–Spittel constitutive model. The objective is to evaluate the potential of machine learning techniques for predicting deformation behavior over a wide range of processing conditions, providing more accurate predictions than traditional phenomenological models.

### 2 Materials and methods

Figure 1 schematically illustrates the steps developed in this work. Initially, the flow curves of the material under different temperature and strain rate conditions were obtained from tensile tests. These results served as the basis for modeling the plastic behavior of the AA 5052-H32 aluminum alloy, employing both the Hensel–Spittel constitutive equation and artificial intelligence-based models. Finally, the performance of the different models was comparatively evaluated. Each of these steps is described in detail in the following sections.

# 2.1 Tensile tests

Table 1 presents the chemical composition of the AA 5052-H32 aluminum alloy with a thickness of 1 mm used in this study. The composition falls within the nominal range reported in the literature [44].

**Table 1** Chemical composition of the 1 mm thick AA 5052-H32 aluminum alloy

Al	Mg	Si	Fe	Cr	Outros
96,9	2,20	0,18	0,31	0,15	0,26

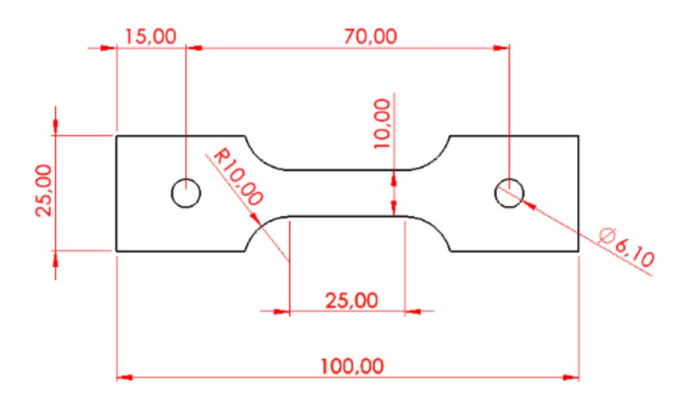


Fig. 2 Detailed geometry of the tensile test specimens

The material was subjected to tensile tests using a Gleeble® 540 thermomechanical simulator. The geometry of the tensile specimen is shown in Fig. 2.

During the tests, the samples were heated to the target temperature at a controlled rate, held at the specified temperature for 30 s to ensure thermal homogenization, and subsequently deformed until fracture. The thermomechanical conditions employed in the hot tensile tests are summarized in Table 2.



Table 2 Thermomechanical parameters of the tensile tests

Condition	Temperature, T [°C]	Strain rate, $\dot{\varphi}$ [1/s]		
1	100	0.01		
2	100	1		
3	200	0,01		
4	200	1		
5	300	0.01		
6	300	1		
7	450	0.01		
8	450	1		

# 2.2 Hensel-Spittel model

A widely employed approach for modeling and predicting flow stress during hot deformation was proposed by Hensel and Spittel [45–47]:

$$k_f = C.e^{m_1.T}.\varphi^{m_2}.\dot{\varphi}^{m_3}.e^{\frac{m_4}{\varphi}}.(1+\varphi)^{m_5.T}.e^{m_7.\varphi}.\dot{\varphi}^{m_8.T}.T^{m_9}$$
 (1)

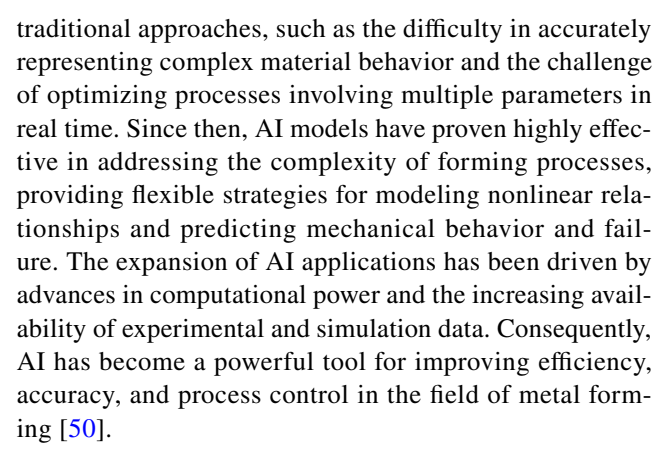
where C,  $m_1$  to  $m_9$  are material constants that must be determined experimentally.

This constitutive model can be regarded as an extension of the classical power-law model, incorporating features of the Hollomon and Swift equations, with the constants expressed as functions of strain and temperature [48]. The Hensel–Spittel model effectively captures the combined effects of strain, strain rate, and temperature on flow stress, and has been shown to reproduce the hot deformation behavior of metallic alloys with high accuracy [49]. Moreover, it is implemented in most commercial finite element (FE) software packages, making the determination of its parameters particularly valuable for providing input data to FE simulations.

In this study, the methodology adopted for fitting the constitutive model was based on linearization of Eq. (1) by applying the natural logarithm, which allowed the sequential determination of the model parameters. By considering certain variables constant, different reduced forms of the equation were derived to isolate the coefficients associated with strain rate, temperature, and strain. Linear regressions were then carried out between the experimental data and the transformed variables, enabling the extraction of the parameters from the average slopes and intercepts obtained under different conditions.

# 2.3 Modeling using artificial intelligence

Artificial Intelligence (AI)-based models began to be applied to metal forming processes in the 1990s. Their introduction aimed to overcome inherent limitations of



Owing to these characteristics, various AI-based approaches have been employed for predicting metal flow curves [51–56]. Unlike phenomenological constitutive models, such as Hensel–Spittel, AI models do not require a priori definition of explicit mathematical relationships between input and output variables, which confers greater flexibility and ease of implementation. However, this also means that the underlying physical relationships are not directly embedded in the model [49].

In this study, two AI-based approaches were investigated: Artificial Neural Networks (ANN) and eXtreme Gradient Boosting (XGBoost). Both models were trained using experimental data obtained from tensile tests on the AA 5052 alloy, where strain, strain rate, and temperature were varied to predict flow stress under different forming conditions.

The methodology began with data preprocessing. The input variables — strain  $(\varphi)$ , strain rate  $(\dot{\varphi})$ , and temperature (T) — and the output variable — flow stress  $(k_f)$  — were organized into a structured dataset. For the ANN model, the Min–Max normalization technique was applied to scale the data between 0 and 1, ensuring balanced variable distributions and improving training stability and convergence.

In the ANN approach, the dataset was divided into training and test subsets, with 20% reserved for final validation. The network architecture was defined through automated hyperparameter optimization, systematically exploring combinations of hidden layers and activation functions based on predictive performance. The final network was trained using the Adam optimizer with mean squared error (MSE) as the loss function. To mitigate overfitting, an early stopping criterion was applied, interrupting training when validation loss did not improve for 30 consecutive epochs.

Throughout training, the model's performance was continuously monitored using metrics such as mean absolute error (MAE) and MSE on both training and validation sets. Learning curves were analyzed to confirm training stability and generalization capability. Once trained, the ANN model was applied to the entire dataset to generate predicted flow curves, which were subsequently compared to the experimental results.



The methodology applied to the XGBoost model followed similar principles. However, this algorithm does not require input normalization and is particularly effective for tabular datasets. Model tuning was performed through crossvalidation combined with optimization of key hyperparameters, including tree depth, learning rate, and the number of estimators. After fine-tuning, the XGBoost predictions were compared with the experimental data, enabling a critical assessment of its predictive accuracy relative to the ANN.

#### 3 Results

This section presents the results obtained in this study, starting with the experimental characterization of the warm and hot mechanical behavior of the AA 5052-H32 alloy and subsequently addressing its modeling using advanced Artificial Intelligence techniques.

# 3.1 Flow curves of the AA 5052-H32 alloy

Figure 3 shows the flow curves of the AA 5052-H32 alloy obtained at different temperatures and strain rates. A pronounced influence of temperature on the material strength is observed. As the deformation temperature increases, the flow stress decreases significantly, reflecting the thermal softening behavior characteristic of metallic materials. This effect is particularly evident when comparing the flow stress at  $100~^{\circ}\text{C}$  ( $\dot{\varphi} = 0.011/s$ ), approximately 185 MPa, with that measured at  $400~^{\circ}\text{C}$  ( $\dot{\varphi} = 0.011/s$ ), only 37 MPa — corresponding to a reduction of about 80%.

The strain rate also influences the flow stress. At all evaluated temperatures, higher strain rates resulted in higher flow stresses, due to the limited action of softening mechanisms, which require time to develop. Consequently, strain hardening becomes more pronounced at

higher strain rates, increasing the resistance to plastic flow. This effect is less significant than that of temperature but becomes more pronounced as temperature rises. While at 100 °C the increase in flow stress is only about 7%, at 450 °C the increment exceeds 32%.

The shape of the flow curves also varies with the thermal condition. At 100 °C, for example, a continuous increase in stress with strain is observed, indicating the strong influence of strain hardening. At intermediate temperatures, such as 300 °C, the stress increase with strain is less pronounced. At 450 °C, the curve exhibits an almost stable plastic region, with little additional increase in flow stress, revealing the dominant role of thermal softening mechanisms. Similar behavior for the AA 5052 alloy under comparable deformation conditions was also reported by [57].

Table 3 presents the mechanical properties obtained from the tensile tests. The influence of temperature and strain rate on the material strength follows the same trend observed in the flow curves. The values of the elastic modulus (E) vary significantly with temperature. At 100 °C, E remains close to 68 GPa, while at 450 °C it decreases to approximately 22 GPa. The results also indicate a tendency for stiffness to increase with higher strain rates, although this effect is considerably less pronounced than that of temperature.

Elongation exhibits an inverse behavior compared to the elastic modulus, increasing with temperature and decreasing with strain rate. The elongation values ranged from 23.8% (100 °C,  $\dot{\varphi} = 11/s$ ) to 47% (450 °C,  $\dot{\varphi} = 0.011/s$ ). Similar results have already been reported by other researchers [57–59].

#### 3.2 Hensel-Spittel model

Table 4 presents the parameters of the Hensel–Spittel constitutive equation obtained from fitting the experimental data.

Fig. 3 Flow stress curves of the AA 5052-H32 alloy obtained under different temperatures and strain rates

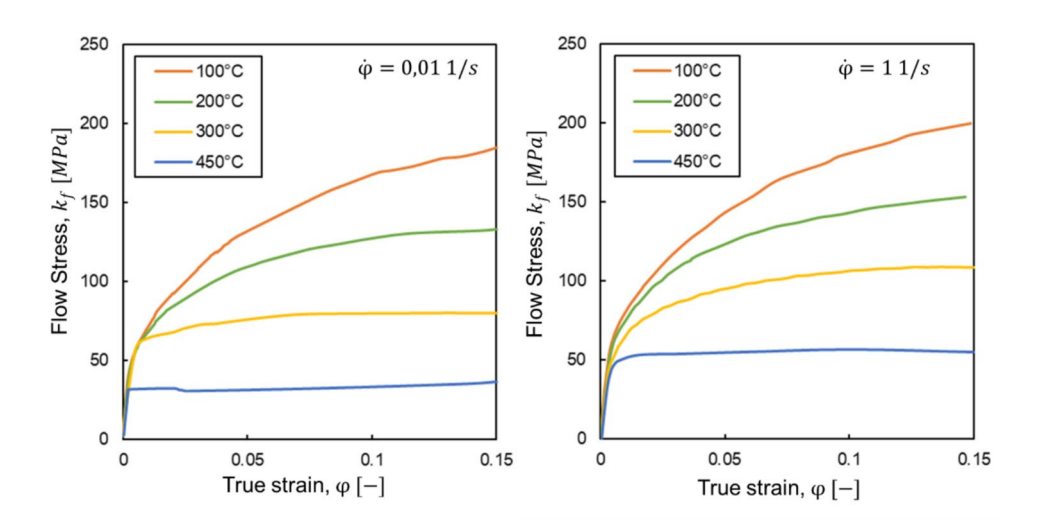




**Table 3** Mechanical properties of the AA 5052-H32 alloy obtained from tensile tests at different temperatures and strain rates

Temperature (°C)	Strain rate (s <sup>-1</sup> )	Elastic modu- lus (GPa)	Yield strength (MPa)	Ultimate tensile strength (MPa)	Elongation (%)
100	0.01	67.0	61.4	160.8	24.8
100	1	68.0	64.5	173.7	23.3
200	0.01	42.6	57.9	115.3	28.6
200	1	44.0	59.1	133.8	26.8
300	0.01	31.2	56.9	69.6	33.0
300	1	32.0	58.0	94.0	32.2
450	0.01	21.5	32.2	32.9	47.0
450	1	23.0	47.3	48.8	45.2

**Table 4** Hensel-Spittel parameters for the AA 5052-H32 alloy

С	$m_1$	$m_2$	$m_3$	$m_4$	$m_5$	$m_7$	$m_8$	$m_9$
1247.7	-8.443	0.872	0.030	0.002	-0.101	-2.129	-0.948	0.572

Figure 4 compares the experimental flow stress curves with those predicted by the model.

Overall, a good agreement was observed between the modeled and experimental data, as illustrated in Fig. 5, which depicts the correlation between predicted and measured flow stress. Although the model achieved a high coefficient of determination (R<sup>2</sup>=0.9847), indicating strong predictive capability, its performance varied with the testing conditions. At higher temperatures, particularly at 450 °C, the model was less effective in capturing the material's behavior, highlighting its limited ability to represent the dominant thermal softening mechanisms. This shortcoming stems from the phenomenological nature of the model, whose parameters are obtained by regression within specific ranges of temperature, strain, and strain rate, thereby restricting its extrapolation. Nevertheless, the Hensel–Spittel model remains advantageous due to its widespread implementation

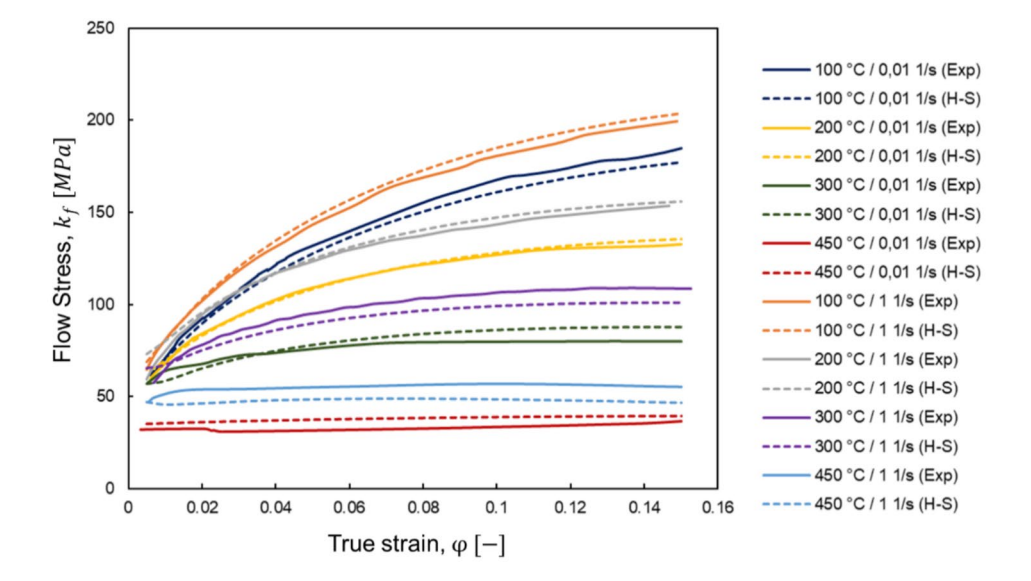
in commercial finite element software, which facilitates direct integration into numerical simulations of forming processes.

Analysis of the coefficients provides further insight into the material behavior. The negative value of parameter  $m_1$  confirms the expected trend of decreasing flow stress with increasing temperature, consistent with the typical thermal softening of metals during hot forming. The positive value of  $m_2$  reflects strain hardening, as evidenced by the gradual increase in strength with true strain.

The influence of strain rate, represented by  $m_3 = 0.0304$ , was found to be minor, indicating low strain-rate sensitivity under the evaluated conditions. The exponential term  $m_4/\varphi$  plays a more significant role at low strains, contributing to the initial increase in flow stress.

The negative value of m<sub>5</sub> modulates the  $(1 + \varphi)$  term, reducing the effect of strain hardening, particularly at

**Fig. 4** Comparison between the experimental and Hensel-Spittel model-predicted flow stress curves of the AA 5052-H32 alloy





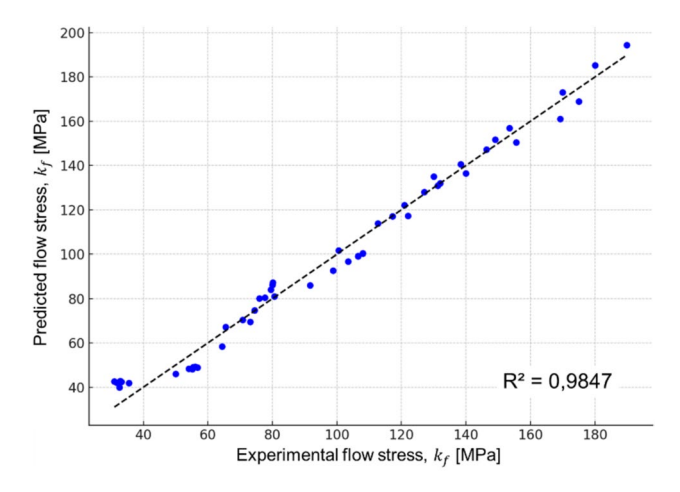


Fig. 5 Comparison between the experimental and Hensel-Spittel model-predicted flow stress data for the AA 5052-H32 alloy

high temperatures. Parameters m<sub>7</sub> and m<sub>8</sub>, both negative, are important for describing thermal softening and dynamic recovery, especially at high strains and elevated temperatures. The positive parameter m<sub>9</sub> compensates for the exponential reduction in strength imposed by m<sub>1</sub>, effectively adjusting the slope of the flow curve as a function of temperature.

#### 3.3 ANN model

The architecture of an Artificial Neural Network (ANN) has a direct impact on its predictive performance [60], particularly in problems involving complex and nonlinear relationships, such as the prediction of flow stress in the AA 5052-H32 alloy. To identify the optimal architecture based on the input variables — strain, strain rate, and temperature — an automated hyperparameter search algorithm was employed. This strategy followed an exhaustive and systematic process in which different combinations of hidden layers and activation functions were evaluated in terms of predictive accuracy.

Several pyramid-structured architectures were manually defined to represent varying levels of network complexity. The main characteristics of these architectures are summarized in Table 5. In addition, three widely used activation functions for regression problems — ReLU, Tanh, and ELU — were tested. The code implements a nested loop in which, for each architecture, all activation functions are systematically combined and evaluated.

For each configuration, a Sequential-type ANN was constructed with the specified hidden layers and activation functions. The model was compiled using the Adam optimizer and mean squared error (MSE) as the loss function. Training was performed with internal validation (validation\_split=0.2) and overfitting control through the EarlyStopping

Table 5 Characteristics of the evaluated ANN architectures

Architecture	Hidden Layers	Total Neurons	Neuron Distribution
[31, 63]	2	96	64→32
[128, 64]	2	192	$128 \rightarrow 64$
[256, 128]	2	384	$256 \rightarrow 128$
[512, 256, 128]	3	896	$512 \rightarrow 256 \rightarrow 128$
[512, 256, 128, 64]	4	960	$512 \rightarrow 256 \rightarrow 128 \rightarrow 64$

technique (patience = 30). Final performance evaluation was conducted on the test set using three metrics: mean absolute error (MAE), mean squared error (MSE), and the coefficient of determination ( $\mathbb{R}^2$ ).

The results from all executions were stored in a list of dictionaries, which was subsequently converted into a Data-Frame. This DataFrame was sorted according to the lowest MSE, allowing an objective identification of the most accurate and robust architectures. Figures 6, 7, and 8 compare the MAE, MSE, and R<sup>2</sup> values for the five best-performing models.

The experimental data exhibit nonlinear and coupled relationships between the input variables. For example, flow stress does not increase linearly with strain and is strongly influenced by strain rate and, most notably, by temperature [41]. The best-performing architectures identified were those with multiple hidden layers organized in a pyramidal structure, with a progressively decreasing number of neurons. This type of architecture enables the extraction of high-level representations from the input variables and promotes good generalization capability by gradually reducing dimensionality and emphasizing the most relevant interactions.

The activation functions ELU and Tanh appeared in the best-performing model combinations. The Exponential Linear Unit (ELU) offers advantages such as smoothness and improved handling of negative gradients, thereby supporting more efficient deep learning [61]. The Tanh function, in turn, is symmetric around zero, which benefits regression tasks and enhances training convergence. The use of these activation functions in deep architectures contributed to more stable training and a better representation of smooth variations in the data [62].

The top-performing architectures achieved a balance between fitting capacity and robustness against overfitting. Very simple networks fail to capture the complexity of the phenomenon, whereas excessively deep networks tend to overfit the data.

Figure 9 illustrates the architecture of the Artificial Neural Network (ANN) selected as the most effective for predicting the flow stress of the AA 5052-H32 alloy. The input layer receives the strain  $(\varphi)$ , strain rate  $(\dot{\varphi})$ , and temperature (T) values, which represent the deformation conditions of the



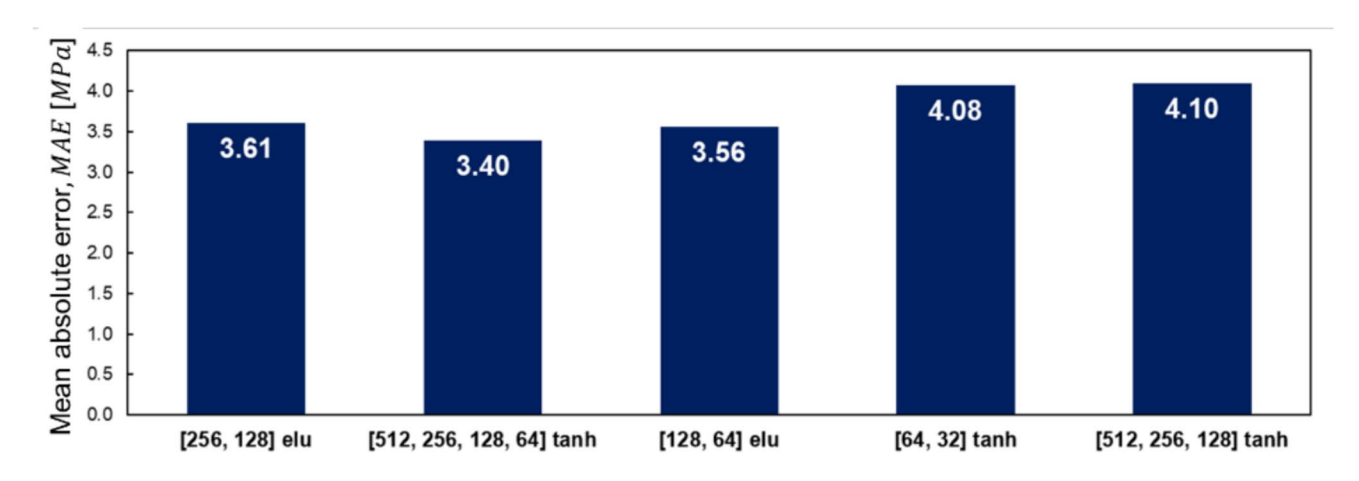


Fig. 6 MAE results for the five best-performing ANN models

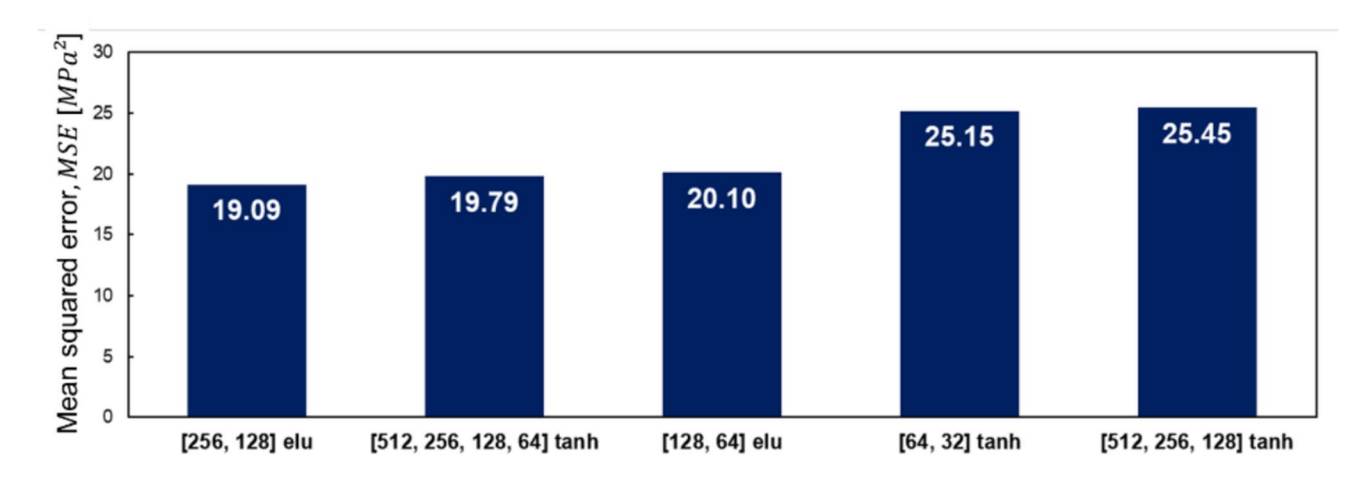


Fig. 7 MSE results for the five best-performing ANN models

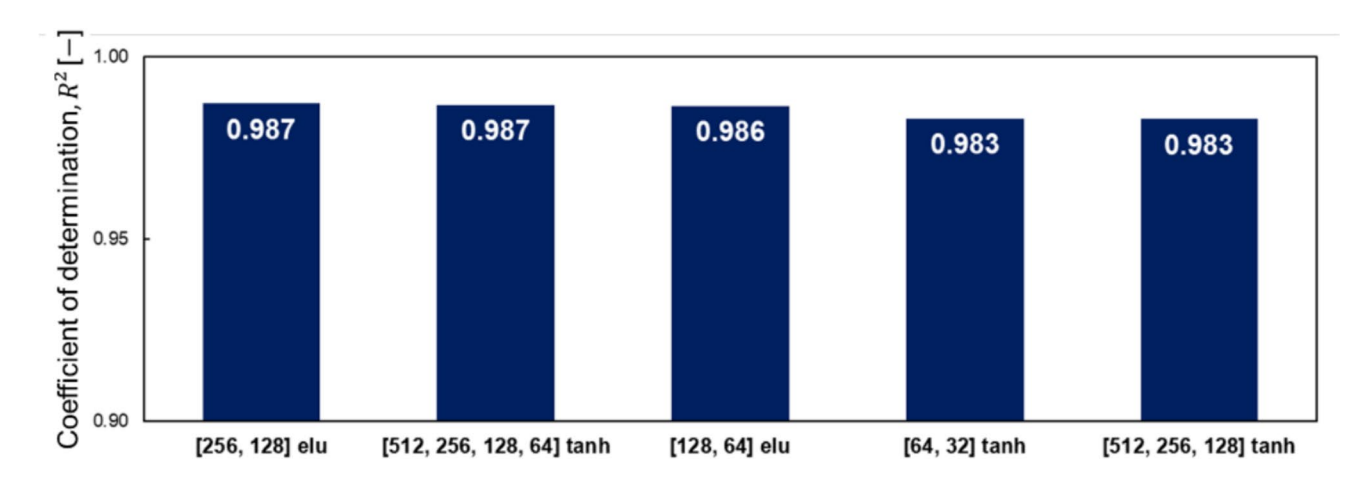


Fig. 8 R<sup>2</sup> results for the five best-performing ANN models



Fig. 9 Schematic diagram of the Hidden layers **Output layer** Input layer ANN architecture True strain φ Strain rate Flow stress **Temperature** 256 neurons 128 neurons MAE training MSE training 0.30 MAF test MSE test Mean squared error,  $MSE~[MPlpha^2]$ 0.14 Mean absolute error, MAE [MPa] 0.10 0.08 0.06

0.04

0.00

Fig. 10 Learning curves of the ANN model showing MAE as a function of the number of epochs

Number of Epochs [-]

0.10

Fig. 11 Learning curves of the ANN model showing MSE as a function of the number of epochs

Number of Epochs [-]

material during tensile testing. These inputs are connected to the first hidden layer, containing 256 neurons. The processed signals are then passed to a second hidden layer with 128 neurons. Both hidden layers employ the Exponential Linear Unit (ELU) activation function. The output layer consists of a single neuron, responsible for generating the predicted flow stress value  $(k_f)$ . All layers are fully connected, meaning that each neuron in one layer is connected to every neuron in the subsequent layer, thereby enabling the network to capture complex interactions among the input variables.

Figures 10 and 11 present the learning curves of the ANN model in terms of MAE and MSE, respectively. The curves display the typical behavior of successful ANN training [63]. During the initial epochs (up to approximately the 20th), a sharp decrease in both training and validation errors is observed, indicating that the model rapidly learned the underlying patterns in the data.

After this point, both errors decrease more gradually and stabilize around epoch 100, with slight natural oscillations, particularly in the validation curve. Such fluctuations are expected in well-tuned ANNs, especially in problems involving experimental data with inherent variability.

The similarity of error values between the training and validation sets indicates that the model exhibits good generalization capability, with no evident signs of overfitting. The selected architecture — consisting of two hidden layers with 256 and 128 neurons, ELU activation, and regularization via EarlyStopping — proved to be well suited to the nature of the dataset, which involves nonlinear relationships among strain, strain rate, and temperature.



175

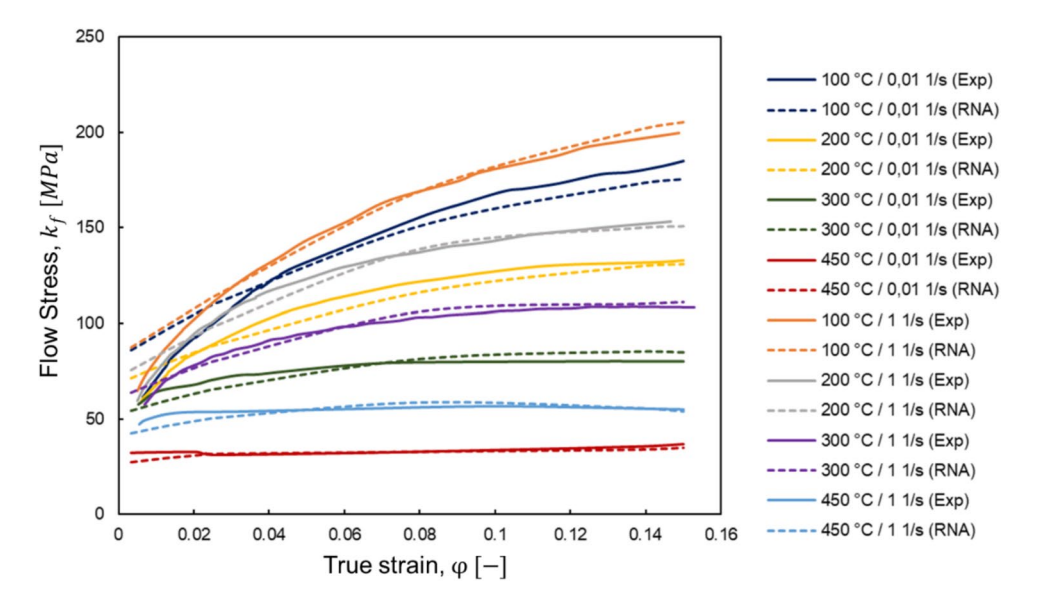
The final performance metrics on the test set were MAE=3.61 MPa and MSE=19.09 MPa<sup>2</sup>, demonstrating the high accuracy of the model and confirming the robustness of the Artificial Neural Network (ANN) in predicting the flow stress of the AA 5052-H32 alloy under different deformation conditions.

Figure 12 reinforces these findings by illustrating the overlap between the experimental flow curves and those predicted by the ANN model, highlighting its ability to accurately capture the alloy's nonlinear behavior. Unlike the Hensel–Spittel model, which exhibited limitations in reproducing the material response at 450 °C, the ANN demonstrated consistent and reliable performance across all test conditions, showing no significant sensitivity to variations in temperature and strain rate.

The robust performance of the ANN proposed in this work is consistent with results previously reported by other researchers [52, 64–66]. Haghdadi et al. [65] developed a high-accuracy artificial neural network model to predict the flow behavior of the A356 aluminum alloy at elevated temperatures. The architecture used by the authors was relatively simple, consisting of only one hidden layer with 20 neurons, which was justified by the restricted temperature range evaluated. In that study, the analysis was focused exclusively on hot-working conditions (400–540 °C).

Moghadam et al. [66] also modeled the plastic deformation of an aluminum alloy under different thermal regimes (warm and hot). The authors achieved excellent predictive performance; however, they proposed two distinct ANN models: one dedicated to lower temperature ranges and another for higher temperatures. The network designed for lower temperatures contained a single hidden layer with 6 neurons, while the network for higher temperatures consisted of two hidden layers with 2 and 4 neurons, respectively.

**Fig. 12** Comparison between the experimental and ANN-predicted flow stress curves of the AA 5052-H32 alloy



In the present work, the mechanical behavior of the AA 5052-H32 alloy under warm and hot forming conditions was modeled using a single ANN. The greater variability of the flow stress curves, resulting from the broader diversity of active deformation mechanisms, required the adoption of a denser architecture, composed of two hidden layers with 256 and 128 neurons. This configuration proved suitable for more accurately capturing the nonlinear relationships among strain, strain rate, and temperature.

# 3.4 eXtreme gradient boosting model

XGBoost is a machine learning algorithm based on gradient boosting that uses decision trees as base learners [67]. It constructs a sequence of trees, where each new tree is trained to correct the residual errors of the previous ones, thereby progressively improving prediction accuracy.

In this study, the XGBoost model was trained to predict the flow stress of the AA 5052-H32 alloy based on experimental data. A configuration with 100 decision trees was employed. Increasing the number of trees generally improves the model's ability to capture complex patterns, but it may also increase the risk of overfitting if other hyperparameters are not properly controlled [68].

The maximum depth of each tree was limited to 4. This parameter controls the number of splits (levels) within a tree. Shallow trees are less likely to overfit the noise in the data, resulting in simpler and more generalizable models. By restricting the depth to 4, the model was encouraged to combine multiple weak learners, thereby enhancing the robustness of the final predictive ensemble.

The learning rate was set to 0.1, meaning that each new tree contributes only 10% of its predictions to the final



output. This parameter functions as a regularization factor, slowing down the learning process and making it more controlled. As a result, the model fits the data more gradually, reducing the likelihood of sudden oscillations or premature overfitting. Although this requires more iterations to converge, it typically yields models with improved generalization capability [69].

Figure 13 schematically illustrates the operation of the XGBoost regression model developed to predict the flow stress of the AA 5052-H32 alloy based on experimental strain  $(\varphi)$ , strain rate  $(\dot{\varphi})$ , and temperature (T) data. During training, the model successively builds 100 decision trees. Each tree may receive a subset of the data and uses the residuals from the previous stage as its new target to improve predictions. D<sub>1</sub>, D<sub>2</sub>, ..., D<sub>n</sub> represent the input data at different boosting stages. Each tree produces a partial prediction of the flow stress (W<sub>1</sub>, W<sub>2</sub>, ..., W<sub>n</sub>), which incrementally corrects the accumulated errors from earlier stages.

The partial predictions from each tree are not summed in full; instead, the model applies a learning rate factor (learning\_rate = 0.1). The weighted sum of all trees results in the final prediction of flow stress.

The learning curves of the XGBoost model, plotted as a function of the number of decision trees (Figs. 14 and 15), show a stable convergence trend for both mean absolute error (MAE) and mean squared error (MSE). After approximately 60 estimators, the errors stabilize, indicating that the model achieves a balance between fitting and generalization.

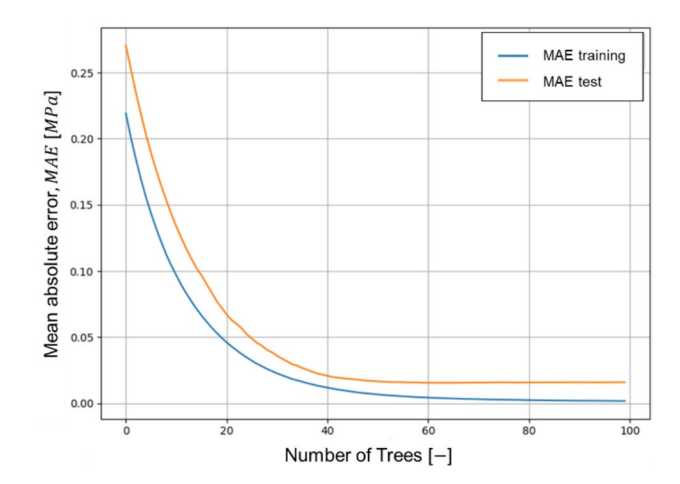
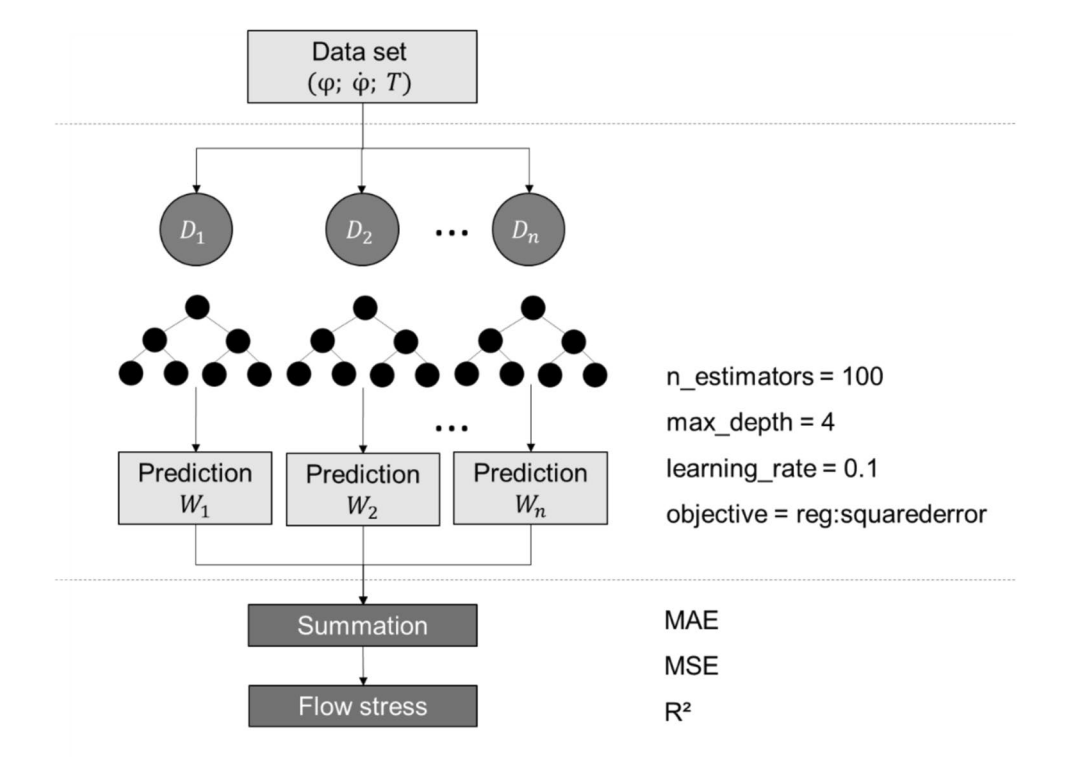


Fig. 14 Learning curves of the XGBoost model showing MAE as a function of the number of decision trees

At the end of training with 100 trees, the model reached MAE=0.7389 MPa and MSE=2.4585 MPa<sup>2</sup> — remarkably low values in the context of flow stress prediction for the AA 5052-H32 alloy. The close agreement between training and validation errors suggests that the model learned efficiently without overfitting, thereby confirming its ability to accurately capture the complex patterns inherent in the experimental data (Fig. 16).

The excellent performance of the model is further evidenced by the scatter plot of actual versus predicted flow stress values (Fig. 15). Most data points are closely

Fig. 13 Schematic diagram of the XGBoost regression model operation





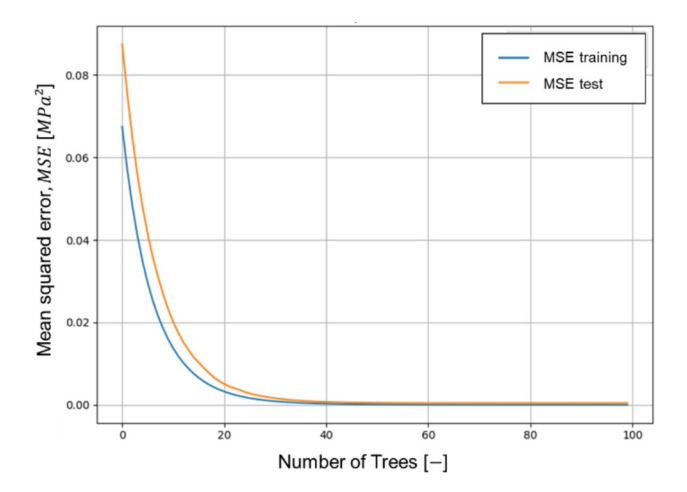


Fig. 15 Learning curves of the XGBoost model showing MSE as a function of the number of decision trees

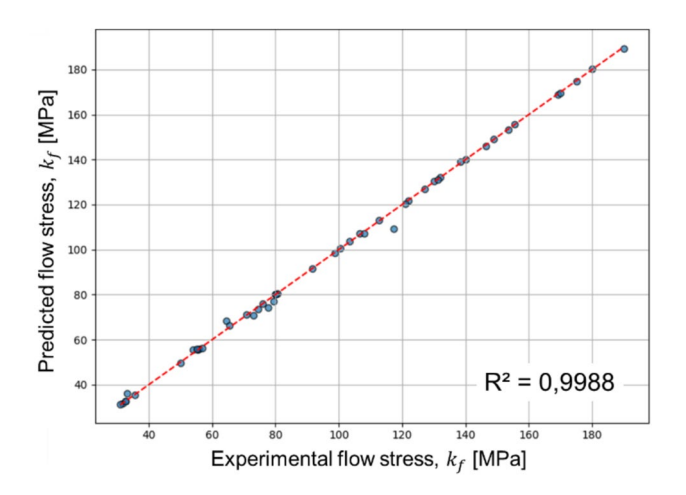
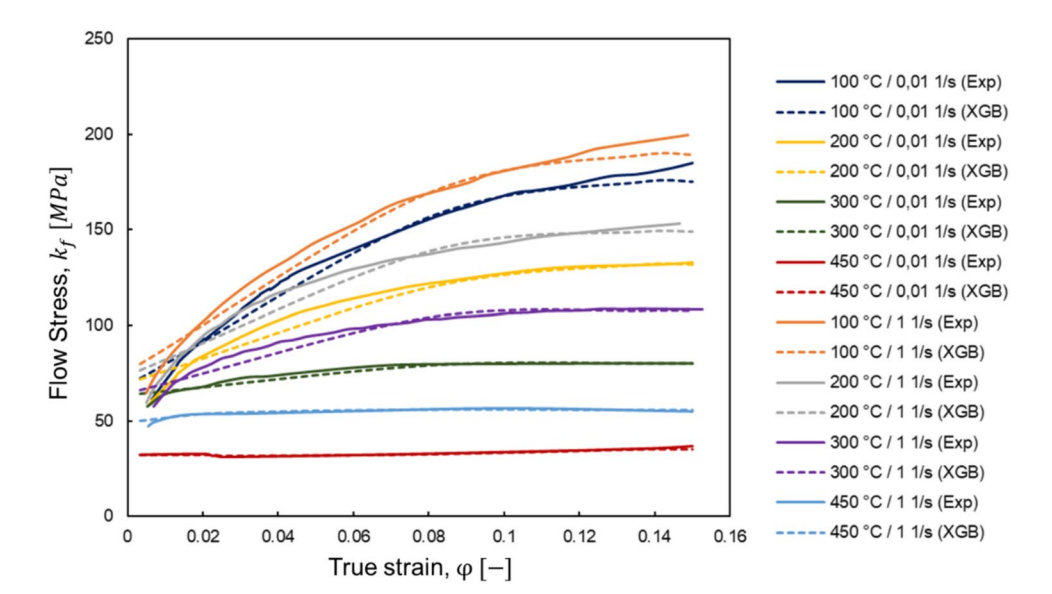


Fig. 16 Scatter plot of actual versus predicted values from the XGBoost model

Fig. 17 Comparison between the experimental and XGBoost model-predicted flow stress curves of the AA 5052-H32 alloy



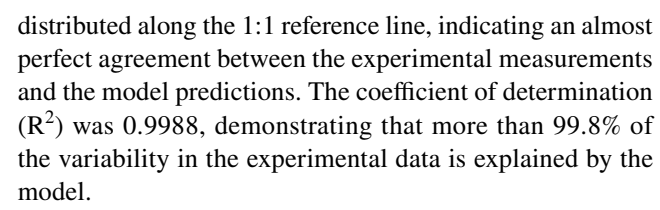


Figure 17 presents the comparison between the experimentally obtained flow stress curves and those predicted by the XGBoost model for the AA 5052-H32 alloy. An excellent alignment is observed between the experimental data and the predicted values, demonstrating the model's high predictive capability across all tested conditions. This performance confirms the robustness and effectiveness of XGBoost as a modeling approach for describing the material's flow behavior, even in the presence of the nonlinear complexity inherent to the relationships among strain, strain rate, and temperature. Similar results were reported by Fan et al. [70], who applied the XGBoost algorithm to model the plastic flow of an austenitic steel alloy under warm and hot deformation conditions.

The outstanding performance of the XGBoost model in predicting flow stress can be attributed to a combination of factors related to both its architecture and the nature of the dataset. First, as a decision tree—based algorithm, it is particularly effective in handling nonlinear relationships such as those present in metallic flow curves. Moreover, XGBoost is recognized for its efficiency even with relatively small datasets, which is especially advantageous in experimental contexts where data availability is often limited [69].

Another key advantage is its ability to capture complex interactions among the input variables  $(\varphi, \dot{\varphi}, T)$ , allowing accurate modeling of their combined influence on the material's strength. Finally, the algorithm incorporates built-in regularization techniques during training, which help prevent



overfitting and enhance generalization capability. These features make XGBoost particularly well suited for predictive problems in materials science and process engineering.

# 4 Conclusions

This study investigated the application of artificial intelligence (AI) techniques to model the deformation behavior of the AA 5052-H32 aluminum alloy under warm and hot forming conditions. The main conclusions are presented below:

AI-based models outperformed the Hensel–Spittel constitutive model. Despite its good accuracy ( $R^2$ =0.9847), the classical model showed limitations at higher temperatures. These results highlight the extrapolation restrictions inherent to phenomenological models.

Artificial Neural Networks (ANNs) achieved robust performance under all evaluated conditions. The optimized dense architecture, composed of two hidden layers (256 and 128 neurons), reached MAE = 3.61 MPa and MSE = 19.09 MPa<sup>2</sup>, adequately reproducing the nonlinear and coupled influence of strain, strain rate, and temperature on flow stress.

The XGBoost model outperformed the other approaches, achieving MAE = 0.74 MPa, MSE = 2.46 MPa<sup>2</sup>, and R<sup>2</sup> = 0.9988, with excellent overlap between experimental and predicted curves. Its ensemble structure of decision trees proved efficient in capturing complex interactions among process variables while maintaining high generalization capability. The results demonstrate the strong robustness of this type of model even with relatively small datasets, a particularly useful feature in metallurgical experiments.

The findings showed that AI-based models can provide higher accuracy and predictive robustness compared to traditional constitutive equations. The integration of AI techniques into material behavior modeling emerges as a promising pathway to expand predictive capacity in mechanical forming process analysis. Future work should consider expanding the dataset with other deformation modes and developing hybrid strategies that combine the physical interpretability of constitutive models with the predictive power of machine learning.

**Acknowledgements** The authors thank CNPq, CAPES and FAPERGS for financial support (FAPERGS/CAPES 06/2018, process: 19/2551-0000710-8);(CNPq/MCTI/FNDCT n° 18/2021, process: 404196/2021-7);(CNPq research productivity – PQ1-4/2021; PDJ – 25/2021 150252/2022-6; GD – 2019); (CNPq process: 309188/2021-0); (CNPq process: 446930/2023-7); (CNPq process: 408298/2023-5); (CAPES (PROEXIES-2020); and the SENAI CIMATEC (Salvador/BA) for technical support.

#### **Declarations**

Conflict of interest The authors certify that they have no affiliations with or involvement in any organization or entity with any financial interest, or non-financial interest in the subject matter or materials discussed in this manuscript.

Ethical approval Not Applicable.

# References

- Abdollahzadeh A, Vanani BB, Koohdar H (2024) Influence of variation ambient system on dissimilar friction stir welding of Al alloy to Mg alloy by the addition of nanoparticles and interlayer. Met Mater Int 30:2830–2852
- Vanani BB, Abdollahzadeh A (2024) Fabrication of reinforced Al-Mg composite by TiC particles via FSW: microstructure and tribology study. J Mater Res Technol 30:6787–6801
- Abdollahzadeh A, Bagheri Vanani B, Koohdar H et al (2024) Multi-pass friction stir welding of Al-TiC-Zn-Mg composite: microstructure and mechanical characteristics. Metallogr Microstruct Anal 13:601–623
- Abdollahzadeh A, Vanani BB, Eivani AR (2024) Advancements in joining Al–Zn–TiC–Mg composites using friction stir welding process: influence of traverse speed. J Compos Mater 58:26
- Lahaye C et al (2009) Contribution of aluminium to the multimaterial light-weight BIW design of SuperLight-Car (SLC). Alum Int Today 21:5
- Aumüller M (2014) Sicherheit und Leichtbau mit AMAG Aluminium. AluReport AMAG TopForm UHS:14–15
- Hirsch J, et al. (2008) Hot forming of aluminium for light-weight car design. Aluminium Int Today 2388–2393
- Akkireddy LA, et al. (2020) Formability studies of automotive aluminium alloy sheet series: A review. E3S Web Conf 184:1–9
- Wu R, Dai W, Luo J, Li M, Liu Y, Li H (2025) Aluminum alloy hot stamping and forming technology: a review. Materials 18:1694
- Toros S, Ozturk F, Kacar I (2008) Review of warm forming of aluminum–magnesium alloys. J Mater Process Technol 207:1–12
- 11. Pradeau A, Thuillier S, Yoon JW (2016) Prediction of failure in bending of an aluminium sheet alloy. Int J Mech Sci 119:23–35
- Georgantzia E, Gkantou M, Kamaris GS (2021) Aluminium alloys as structural material: a review of research. Eng Struct 227:111372
- Tisza M, Czinege I (2018) Comparative study of the application of steels and aluminium in lightweight production of automotive parts. Int J Lightweight Mater Manuf 1:229–238
- Zheng K, Politis DJ, Wang L (2018) A review on forming techniques for manufacturing lightweight complex-shaped aluminium panel components. Int J Lightweight Mater Manuf 1:55–80
- Zhang R, Wang W, Lin J, Dean TA (2023) An indirect hot form and quench (HFQ) for manufacturing components of aluminum alloy sheets and comparison with direct HFQ. Int J Mach Tools Manuf 192:104073
- Lee J, Bong HJ, Kim D et al (2019) Application of combined W-temper and cold forming technology to high-strength aluminum alloy automotive parts. JOM 71:4393

  –4404
- Milkereit B, Österreich M, Schuster P, Kirov G, Mukeli E, Kessler O (2024) Dissolution and precipitation behavior for hot forming of 7021 and 7075 aluminum alloys. Metals 14:1–12
- Shabadi R, Suwas S, Kumar S, Roven HJ, Dwarkadasa ES (2012) Texture and formability studies on AA7020 Al alloy sheets. Mater Sci Eng A 558:439–445



- Dong H, Li X, Li Y, Wang Y, Wang H, Peng X, Li D (2022) A review of electrically assisted heat treatment and forming of aluminum alloy sheet. Int J Adv Manuf Technol 120:7079–7099
- Sun HT, Wang J, Shen GZ, Hu P (2013) Application of warm forming aluminum alloy parts for automotive body based on impact. Int J Automot Technol 14:605–610
- Satish DR, Feyissa F, Kumar DR (2017) Cryorolling and warm forming of AA6061 aluminum alloy sheets. Mater Manuf Process 32:1345–1352
- Polak S, Kaczyński P, Gronostajski Z, Jaskiewicz K, Krawczyk J, Skwarski M, Zwierzchowski M, Chorzępa W (2017) Warm forming of 7075 aluminum alloys. Procedia Eng 207:2399–2404
- Palumbo G, Tricarico L (2007) Numerical and experimental investigations on the warm deep drawing process of circular aluminum alloy specimens. J Mater Process Technol 184:115–123
- Fan X, He Z, Yuan S, Lin P (2013) Investigation on strengthening of 6A02 aluminum alloy sheet in hot forming-quenching integrated process with warm forming-dies. Mater Sci Eng A 587:221-227
- 25. Gao H, Weng T, Liu J, Li C, Li Z, Wang L (2016) Hot stamping of an Al–Li alloy: a feasibility study. Manuf Rev 3:9
- Ju L, Altan T (2015) Forming Al alloys at elevated temperatures. Stamping J 2015:1–6
- Zhou J et al (2014) Forming defects in aluminum alloy hot stamping of side-door impact beam. Trans Nonferrous Met Soc China 24:11
- Harrison NR, Luckey SG (2014) Hot stamping of a B-pillar outer from high strength aluminum sheet AA7075. SAE Tech Pap 2014–01–0981
- Liu Y, Zhu Z, Wang Z (2018) Flow and friction behaviors of 6061 aluminum alloy at elevated temperatures and hot stamping of a B-pillar. Int J Adv Manuf Technol 96:4063–4083
- Brünger E, Engler O, Hirsch J (2006) Al-Mg-Si sheet for autobody application. Virtual Fabrication of Aluminium Products. Wiley-VCH Verlag, Weinheim, pp 51–61
- El Mehtedi M, Spigarelli S, Gabrielli F, Donati L (2015) Comparison study of constitutive models in predicting the hot deformation behavior of AA6060 and AA6063 aluminium alloys.
   Mater Today Proc 2:4732–4739
- 32. Li J, Li F, Cai J, Wang R, Yuan Z, Xue F (2012) Flow behavior modeling of the 7050 aluminum alloy at elevated temperatures considering the compensation of strain. Mater Des 35:1–7
- Ashtiani HRR, Parsa MH, Bisadi H (2012) Constitutive equations for elevated temperature flow behavior of commercial purity aluminum. Mater Sci Eng A 545:61–67
- Haghdadi N, Zarei-Hanzaki A, Abedi HR (2012) The flow behavior modeling of cast A356 aluminum alloy at elevated temperatures considering the effect of strain. Mater Sci Eng A 552:540–545
- Lin YC, Xia YC, Chen XM, Chen MS (2010) Constitutive descriptions for hot compressed 2124–T851 aluminum alloy over a wide range of temperature and strain rate. Comput Mater Sci 48:1092–1097
- Soranansri P, Dubois A, Moreau P (2024) Identification of coulomb and constant shear frictions in hot aluminum forming by using warm and hot upsetting sliding test. Int J Mater Form 17:55
- Liang Z, Zhang Q, Niu L et al (2019) Hot deformation behavior and processing maps of as-cast hypoeutectic Al–Si–Mg alloy. J Mater Eng Perform 28:4871–4881
- Xu J, Su J, Li Y et al (2015) Thermal effects in magnetic pulse forming of magnesium alloy sheet. Int J Adv Manuf Technol 81:755-770

- Tari DG, Worswick MJ (2015) Elevated temperature constitutive behavior and simulation of warm forming of AZ31B. J Mater Process Technol 221:40–55
- He D, Chen SB, Lin YC, Xie H, Li C (2023) Hot tensile behavior of a 7046-aluminum alloy: fracture mechanisms and constitutive models. Mater Today Commun 34:105209
- Rosiak A, Schmeling M, Marcelino R et al (2024) Machine learning applied to predict the flow curve of steel alloys. Int J Adv Manuf Technol 134:5481–5492
- Sheikh H, Serajzadeh S (2008) Estimation of the flow stress behavior of AA5083 using artificial neural networks with respect to dynamic strain aging. J Mater Process Technol 196:115–119
- 43. Yan J, Pan QL, Li AD, Song WB (2017) Flow behavior of Al-6.2Zn-0.70Mg-0.30Mn-0.17Zr alloy during hot compression deformation based on Arrhenius and ANN models. Trans Nonferrous Met Soc China 27:638-647
- Zhou J, Zhang J, Ma M (2017) Study on the formability of aluminum alloy sheets at room and elevated temperatures. Mater Sci Forum 877:393–399
- Gao S, Sang Y, Li Q, Sun Y, Wu Y, Wang H (2022) Constitutive modeling and microstructure research on the deformation mechanism of Ti-6Al-4V alloy under hot forming condition. J Alloys Compd 892:162128
- Chen Y, Li H, Zhang S, Luo J, Teng J, Lv Y, Li M (2023) Hot tensile deformation behavior and constitutive models of GH3230 superalloy double-sheet. Materials 16:803
- 47. El Mehtedi M, Musharavati F, Spigarelli S (2014) Modelling of the flow behaviour of wrought aluminium alloys at elevated temperatures by a new constitutive equation. Mater Des 54:869–873
- Yoo JD, Kim MC, Kim EJ, Razali MK, Joun MS (2021) Flow stress characterization of magnesium alloys at elevated temperatures: a review. J Phys Conf Ser 2047:012002
- Savaedi Z, Motallebi R, Mirzadeh H (2022) A review of hot deformation behavior and constitutive models to predict flow stress of high-entropy alloys. J Alloys Compd 903:163964
- Cao J, Bambach M, Merklein M, Mozaffar M, Xue T (2024) Artificial intelligence in metal forming. CIRP Ann 73:561–587
- Opěla P, Schindler I, Kawulok P, Kawulok R, Rusz S, Rodak K (2019) Hot flow curve description of CuFe2 alloy via different artificial neural network approaches. J Mater Eng Perform 28:4863–4870
- 52. Sani SA, Ebrahimi GR, Vafaeenezhad H, Kiani-Rashid AR (2018) Modeling of hot deformation behavior and prediction of flow stress in a magnesium alloy using constitutive equation and artificial neural network (ANN) model. J Magnesium Alloys 6:134–144
- Ahmadi H, Ashtiani HR, Heidari M (2018) A comparative study of phenomenological, physically-based and artificial neural network models to predict the hot flow behavior of API 5CT-L. J Mater Process Technol 262:1–12
- Mandal S, Sivaprasad PV, Venugopal P (2007) Capability of a feed-forward artificial neural network to predict the constitutive flow behavior of as-cast 304 stainless steel under hot deformation. J Eng Mater Technol 129:242–247
- Lin YC, Zhang J, Zhong J (2008) Application of neural networks to predict the elevated temperature flow behavior of a low alloy steel. Comput Mater Sci 43:752–758
- Mirzadeh H, Cabrera JM, Najafizadeh A (2012) Modeling and prediction of hot deformation flow curves. Metall Mater Trans A 43:108–123
- 57. Li Y, Dong W, Lin Q, Wang Z (2021) Constitutive model and plate forging ability of 5052 aluminum alloy under different temperatures. In: Daehn G, et al. (eds) Forming the Future. The Minerals, Metals & Materials Series. Springer, Cham, pp 1–8



- 58. Summers PT, Chen Y, Rippe CM, Allen B, Mouritz AP, Case SW, Lattimer BY (2015) Overview of aluminum alloy mechanical properties during and after fires. Fire Sci Rev 4:3
- Gu R, Liu Q, Chen S et al (2019) Study on high-temperature mechanical properties and forming limit diagram of 7075 aluminum alloy sheet in hot stamping. J Mater Eng Perform 28:7259–7272
- Wang Y, Wu X, Li X, Xie Z, Liu R, Liu W, Zhang Y, Xu Y, Liu C
   (2020) Prediction and analysis of tensile properties of austenitic stainless steel using artificial neural network. Metals 10:234
- Çatalbaş B, Morgül Ö (2023) Deep learning with extended exponential linear unit (DELU). Neural Comput Appl 35:22705–22724
- 62. Wang Y, Li Y, Song Y, Rong X (2020) The influence of the activation function in a convolution neural network model of facial expression recognition. Appl Sci 10:1897
- Fernández DM, Rodriguez-Prieto A, Xamacho AM (2020) Prediction of the bilinear stress–strain curve of aluminum alloys using artificial intelligence and big data. Metals 10:904
- Haghdadi N, Zarei-Hanzaki A, Khalesian AR, Abedi HR (2013)
   Artificial neural network modeling to predict the hot deformation behavior of an A356 aluminum alloy. Mater Des 49:386–391
- Moghadam NN, Serajzadeh S (2023) Warm and hot deformation behaviors and hot workability of an aluminum–magnesium alloy using artificial neural network. Mater Today Commun 35:105986
- Chen T, Guestrin C (2016) XGBoost: A scalable tree boosting system. Proc 22nd ACM SIGKDD Int Conf Knowl Discov Data Min 785–794

- Nguyen HD, Dao ND, Shin M (2021) Prediction of seismic drift responses of planar steel moment frames using artificial neural network and extreme gradient boosting. Eng Struct 242:112518
- Bentéjac C, Csörgő A, Martínez-Muñoz G (2021) A comparative analysis of gradient boosting algorithms. Artif Intell Rev 54:1937–1967
- Liu Y, Li HY, Su XJ (2013) Artificial neural network modelling to predict hot deformation behaviour of zinc–aluminium alloy. Mater Sci Technol 29:194–200
- Fan M, Zhou H, Peng W et al (2025) Hot compression deformation, constitutive model, and microstructure evolution of austenitic-TWIP/martensitic-HFS composite steel. Met Mater Int. https://doi.org/10.1007/s12540-025-01934-7

**Publisher's Note** Springer Nature remains neutral with regard to jurisdictional claims in published maps and institutional affiliations.

Springer Nature or its licensor (e.g. a society or other partner) holds exclusive rights to this article under a publishing agreement with the author(s) or other rightsholder(s); author self-archiving of the accepted manuscript version of this article is solely governed by the terms of such publishing agreement and applicable law.

